Supplementary Material to
No solid evidence for an inner core on Mars

M. Visser[1], F. D. Munch[1], A. Khan[2], D. A. Frost[3], D. Giardini[1]

[1]Institute of Geophysics, ETH Zurich, Zurich, Switzerland
[2]Institute of Geochemistry and Petrology, ETH Zurich, Zurich, Switzerland
[3]School of the Earth Ocean and Environment, University of South Carolina, Columbia, SC, USA

Corresponding author: F. D. Munch, `federico.munch@eaps.ethz.ch`

Corresponding author: A. Khan, `amir.khan@eaps.ethz.ch`

Contents of this file

1. Figures S1–S8
2. Tables S1

Event listing

Event	Δ [°]	BAZ [°]	Quality
S0173a	31.3 ± 0.9	88 ± 10	B
S0235b	30.4 ± 1.4	77 ± 13	A
S0290b	30.4 ± 8.2		A
S0325a	40.8 ± 1.7	57 ± 15	B
S0409d	28.2 ± 1.8	70 ± 20	A
S0474a	29.1 ± 17.5	96.9	B
S0484b	30.6 ± 3.1	100 ± 20	B
S0784a	30.5 ± 1.6	115 ± 21	A
S0802a	31.4 ± 3	82 ± 14	B
S0809a	30.9 ± 1.6	91 ± 9	A
S0820a	31.4 ± 3.1	106 ± 21	A
S0864a	30.8 ± 1.5	90 ± 22	B
S0916d	29.3 ± 5.9	96.9	A
S0918a	27.8 ± 6.7	136.8	A
S1012d	38.3 ± 3.3		A
S1015f	27.5 ± 2	89	B
S1022a	30.7 ± 2.2	63 ± 5	B
S1039b	30.4 ± 17.5		B
S1048d	30.2 ± 1.3	97 ± 17	B
S1133c	30 ± 1.2	91 ± 13	A
S1157a	35.6 ± 2.5		B
S1197a	32 ± 1.5		B
S1222a	37 ± 1.6	100.9	B

Table S1. Epicentral distances (Δ) and back-azimuth (BAZ) for the highest-quality events that occurred in and around Cerberus Fossae (see map in Figure **??**) and that are considered in this study. Epicentral distances are taken from Khan et al. (2023) and InSight Marsquake Service (2023), whereas the BAZ and quality labels are from the latest marsquake catolog (InSight Marsquake Service, 2023).

11 ## Application to PP

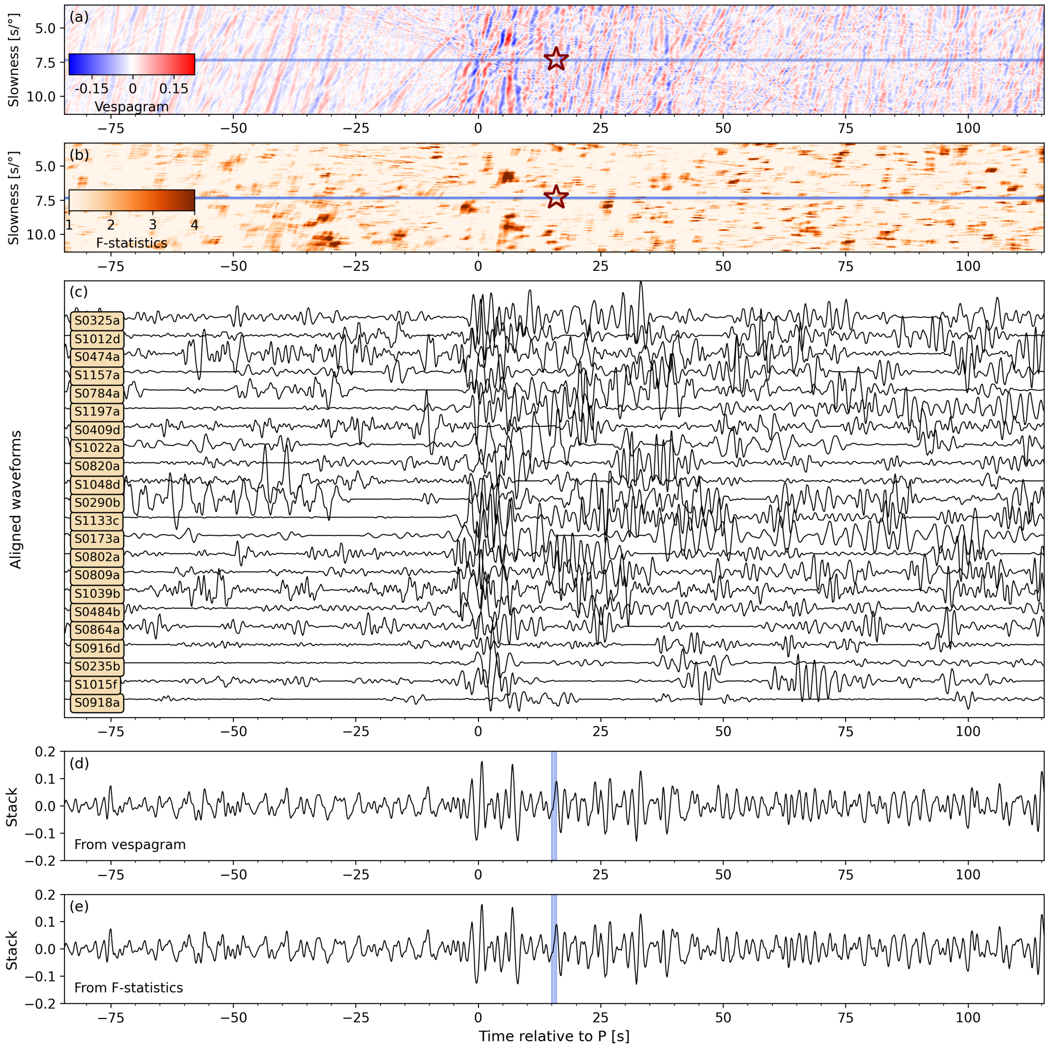

Figure S1. Summary of vespagram and F-statistic analysis applied to the surface reflection body wave phase PP. (a) Vespagram; (b) F-statistic; (c) normalized waveforms aligned based on slowness picked on the vespagram; (d) stacked waveforms based on vespagram; and (e) stacked waveforms based on F-statistic. Red stars on panels (a) and (b) denote the picked slownesses used to generate the waveform stacks in panels (d) and (e), respectively. Times are relative to the predicted P-wave arrival for the reference distance (31°) and velocity model (mean model shown in figure 1). The light blue horizontal (a,b) and vertical (d,e) bars indicate the expected PP slowness and arrival time windows, respectively, for the mantle models of Khan et al. (2023), including uncertainties in event distances.

Application to PPP

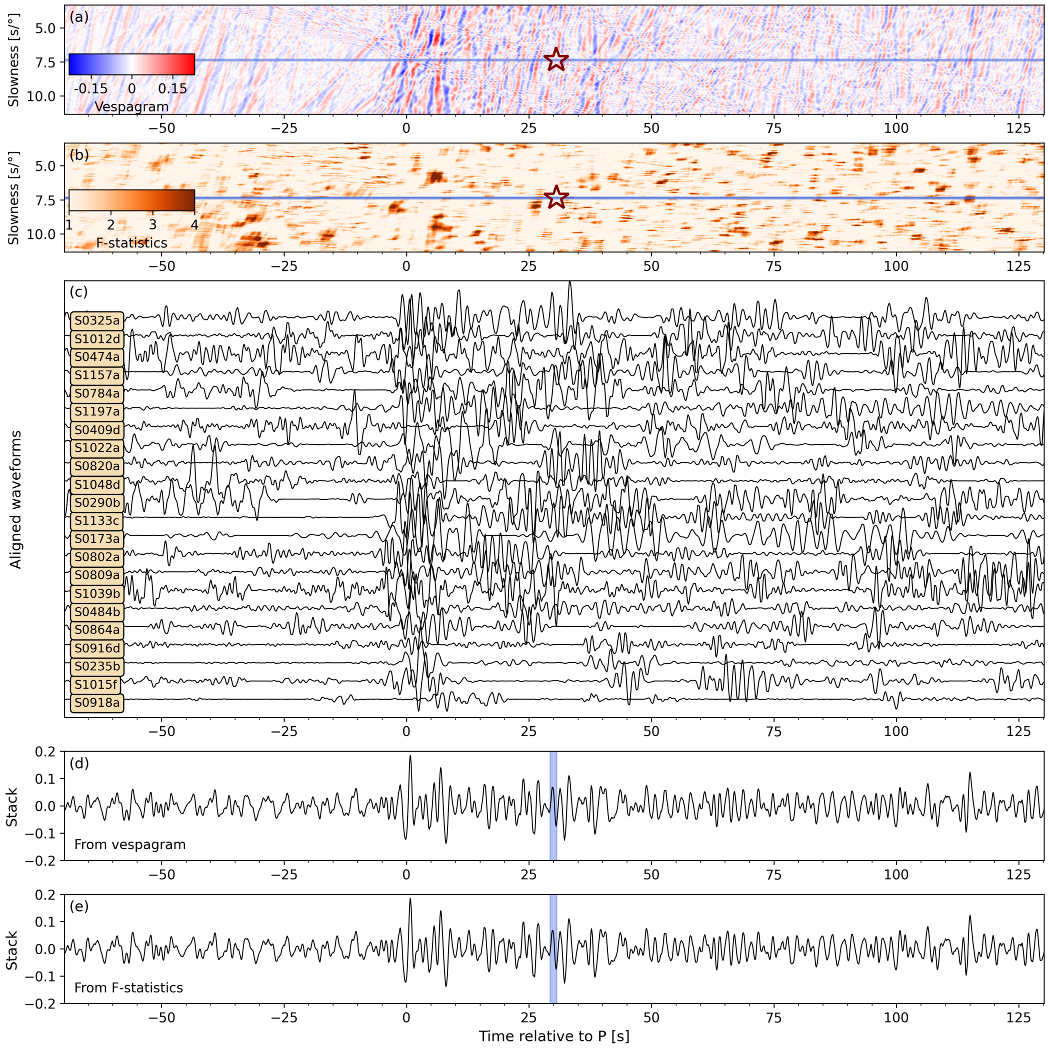

Figure S2. Summary of vespagram and F-statistic analysis applied to the surface reflection body wave phase PPP. (a) Vespagram; (b) F-statistic; (c) normalized waveforms aligned based on slowness picked on the vespagram; (d) stacked waveforms based on vespagram; and (e) stacked waveforms based on F-statistic. Red stars on panels (a) and (b) denote the picked slownesses used to generate the waveform stacks in panels (d) and (e), respectively. Times are relative to the predicted P-wave arrival for the reference distance (31°) and velocity model (mean model shown in figure 1). The light blue horizontal (a,b) and vertical (d,e) bars indicate the expected PPP slowness and arrival time windows, respectively, for the mantle models of Khan et al. (2023), including uncertainties in event distances.

Application to SSS

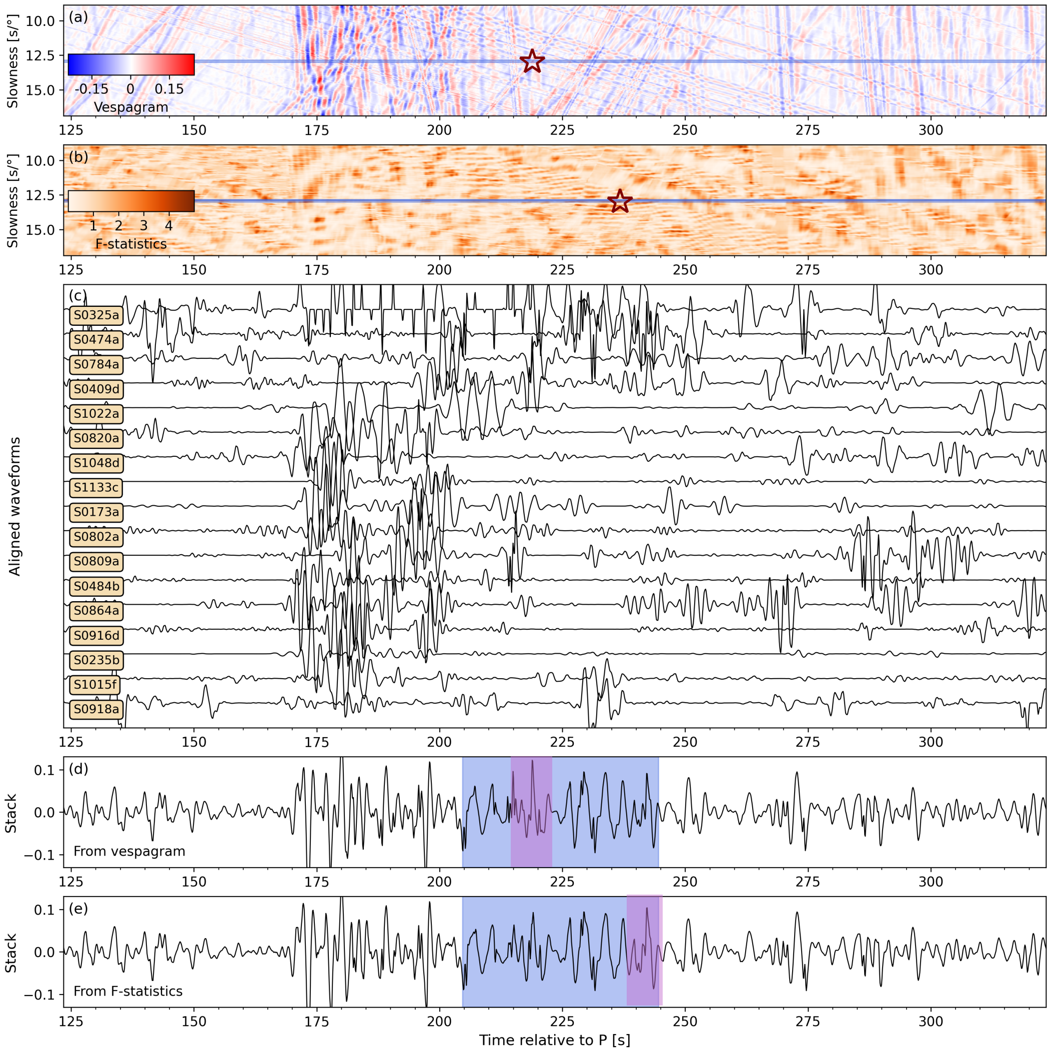

Figure S3. Summary of vespagram and F-statistic analysis applied to the surface reflection body wave phase SSS. (a) Vespagram; (b) F-statistic; (c) normalized waveforms aligned based on slowness picked on the vespagram; (d) stacked waveforms based on vespagram; and (e) stacked waveforms based on F-statistic. Red stars on panels (a) and (b) denote the picked slownesses used to generate the waveform stacks in panels (d) and (e), respectively. Times are relative to the predicted P-wave arrival for the reference distance (31°) and velocity model (mean model shown in figure 1). The light blue horizontal (a,b) and vertical (d,e) bars indicate the expected SS slowness and arrival time windows, respectively, for the mantle models of Khan et al. (2023), including uncertainties in event distances. Magenta-shaded windows indicate energy bursts consistent with SSS-wave arrival based on vespagrams and F-vespagram. We find that the arrival is not coherent between the two diagnostics.

Application to SdS

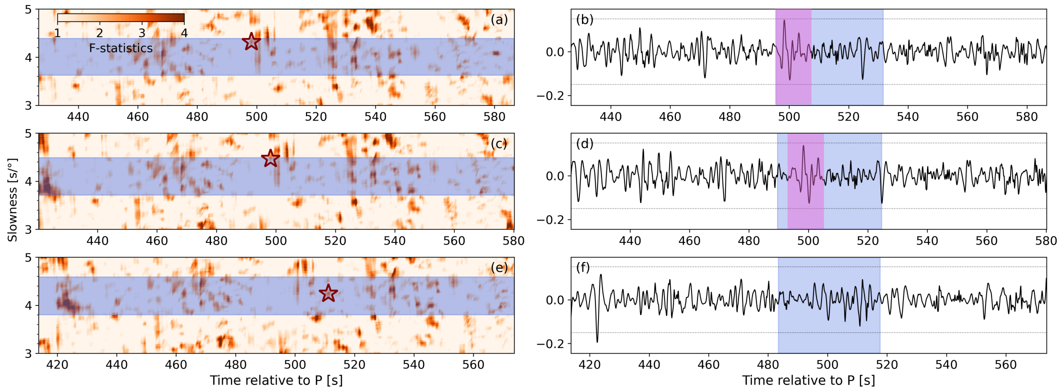

Figure S4. SdS F-vespagram (left) and corresponding stacked waveforms (right) computed for 23 marsquakes with epicentral distances in the range 30°–40° (Table S1), assuming hypothetical solid mantle—molten silicate layer boundary radii of (a-b) 1885 km; (c-d) 1905 km; and (e-f) 1925 km. On each F-statistic, the red star denotes the picked slowness used to generate the waveform stack (righthand panels). Times are relative to the predicted P-wave arrival for the reference distance (31°) and velocity model (shown in figure 1 in the main manuscript). The light blue shading highlights the expected SdS slowness window (horizontal blue bars, lefthand panels) and arrival time window (vertical blue bars, righthand panels) for each solid mantle—molten silicate layer boundary radius, accounting for mantle variability across the velocity models of Khan et al. (2023) and uncertainties in the epicentral distance of the events. Light magenta shaded windows highlight observed energy bursts consistent with potential solid mantle—molten silicate layer boundary reflections.

15 ## Application to PKiKP

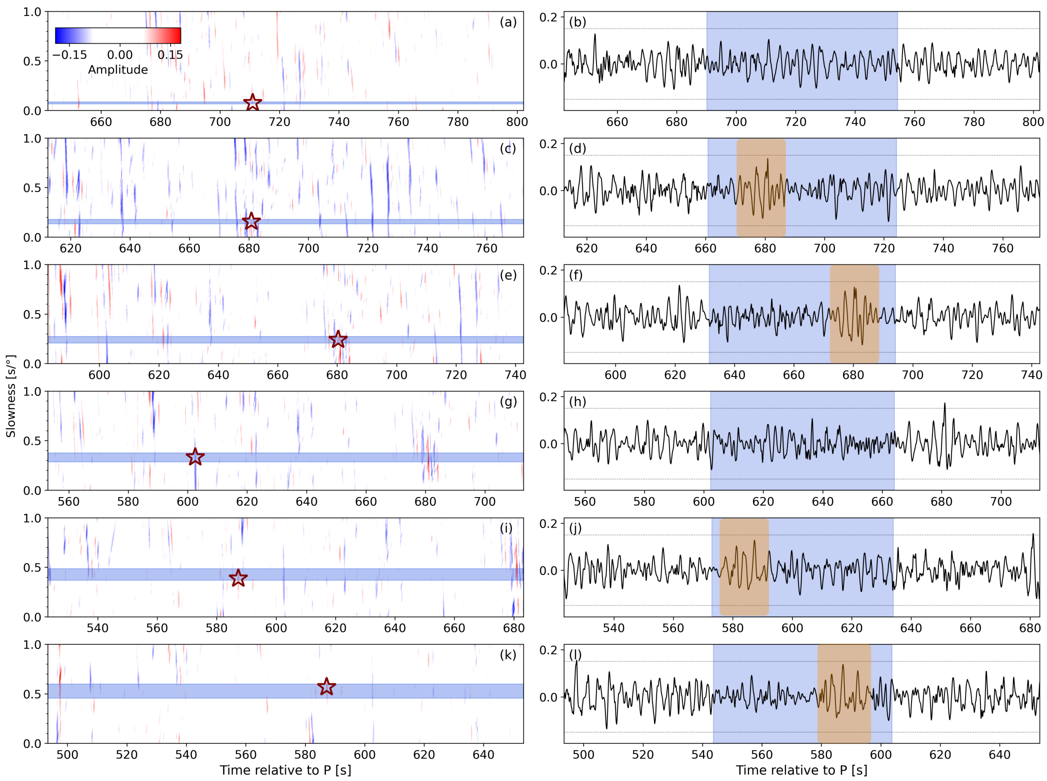

Figure S5. PKiKP vespagram (left) and corresponding stacked waveforms (right) computed for 23 marsquakes with epicentral distances in the range 30°–40° (Table S1), assuming hypothetical inner core radii of (a-b) 100 km; (c-d) 200 km; (e-f) 300 km; (g-h) 400 km; (i-j) 500 km; and (k-l) 600 km. On each vespagram, the red star denotes the picked slowness used to generate the waveform stack (righthand panels). Times are relative to the predicted P-wave arrival for the reference distance (31°) and velocity model (shown in figure 1 in the main manuscript). The light blue shading highlights the expected PKiKP slowness window (horizontal blue bars, lefthand panels) and arrival time window (vertical blue bars, righthand panels) for each inner core radius, accounting for mantle variability across the velocity models of Khan et al. (2023) and uncertainties in the epicentral distance of the events. Light orange shaded windows highlight observed energy bursts consistent with potential inner core reflections.

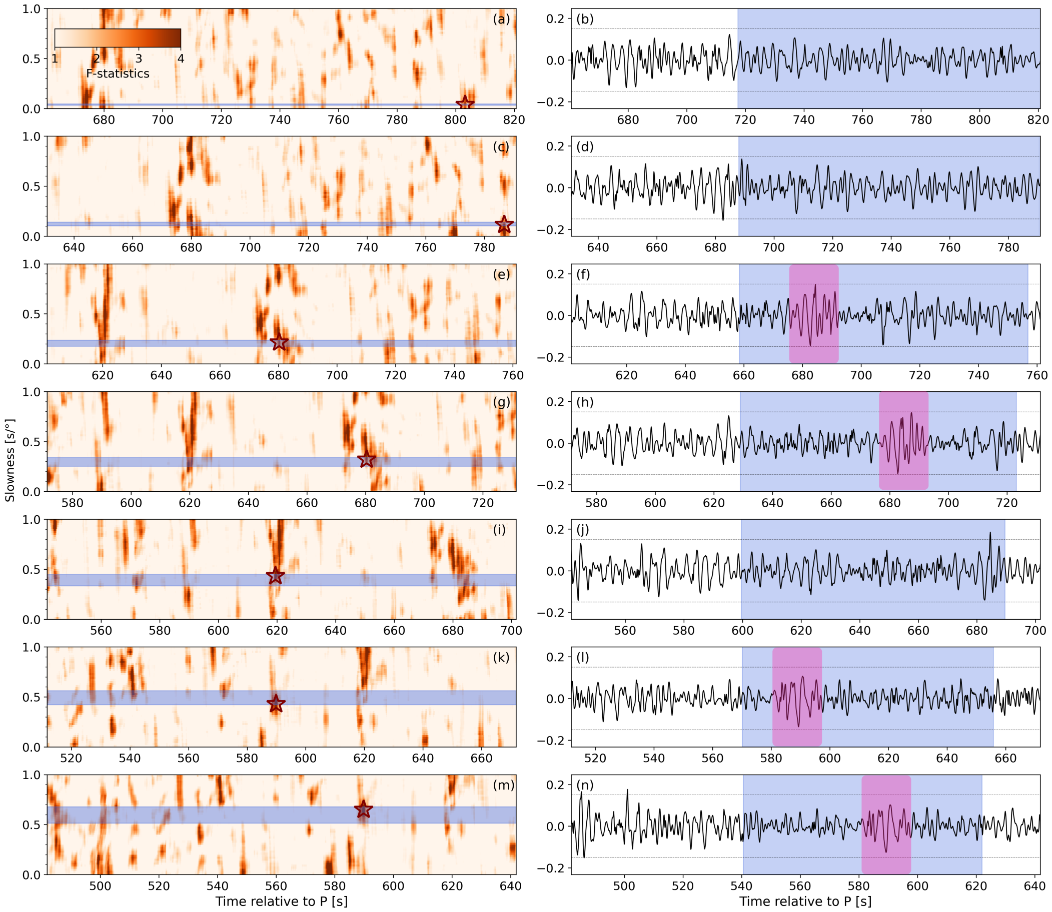

Figure S6. PKiKP F-vespagram (left) and corresponding stacked waveforms (right) computed for 23 marsquakes with epicentral distances in the range 30°–40° (Table S1), assuming hypothetical inner core radii of (a-b) 50 km; (c-d) 150 km; (e-f) 250 km; (g-h) 350 km; (i-j) 450 km; (k-l) 550 km; and (m-n) 650 km. On each vespagram, the red star denotes the picked slowness used to generate the waveform stack (righthand panels). Times are relative to the predicted P-wave arrival for the reference distance (31°) and velocity model (shown in figure 1 in the main manuscript). The light blue shading highlights the expected PKiKP slowness window (horizontal blue bars, lefthand panels) and arrival time window (vertical blue bars, righthand panels) for each inner core radius, accounting for mantle variability across the velocity models of Khan et al. (2023) and uncertainties in the epicentral distance of the events. Light magenta shaded windows highlight observed energy bursts consistent with potential inner core reflections.

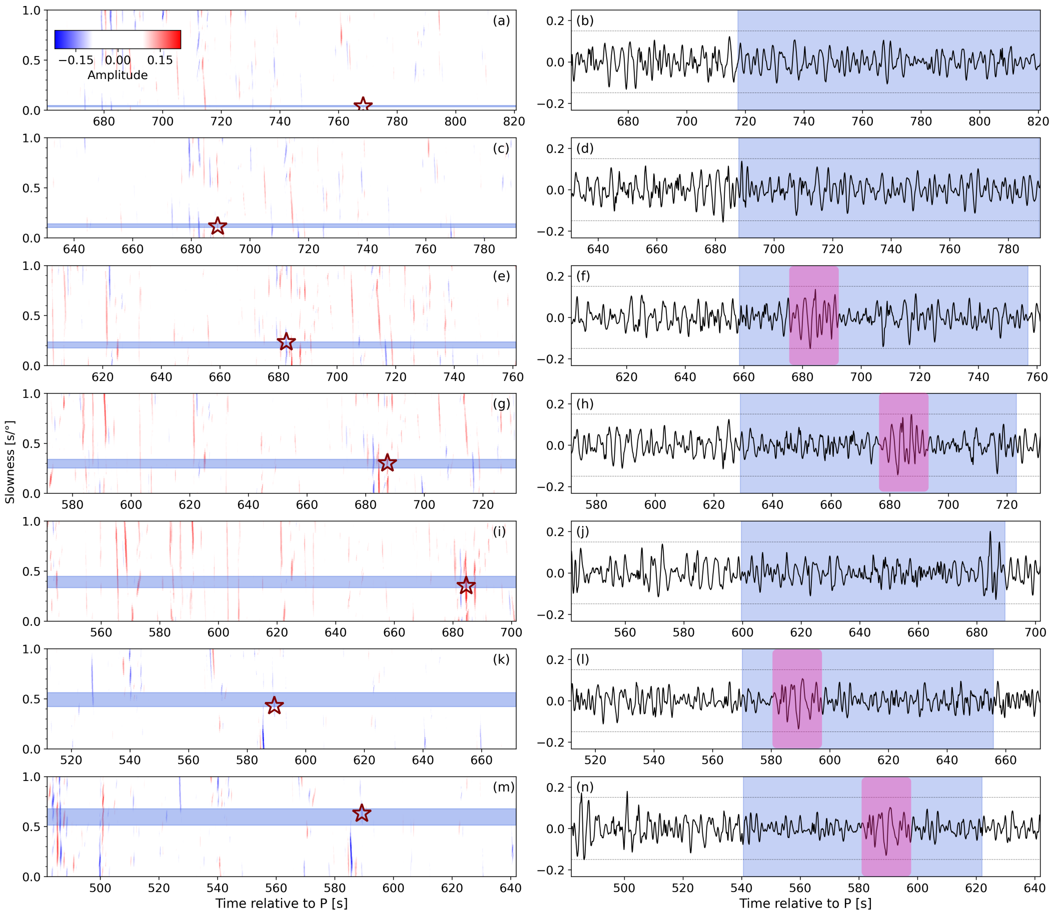

Figure S7. PKiKP vespagram (left) and corresponding stacked waveforms (right) computed for 23 marsquakes with epicentral distances in the range 30°–40° (Table S1), assuming hypothetical inner core radii of (a-b) 50 km; (c-d) 150 km; (e-f) 250 km; (g-h) 350 km; (i-j) 450 km; (k-l) 550 km; and (m-n) 650 km. On each vespagram, the red star denotes the picked slowness used to generate the waveform stack (righthand panels). Times are relative to the predicted P-wave arrival for the reference distance (31°) and velocity model (shown in figure 1 in the main manuscript). The light blue shading highlights the expected PKiKP slowness window (horizontal blue bars, lefthand panels) and arrival time window (vertical blue bars, righthand panels) for each inner core radius, accounting for mantle variability across the velocity models of Khan et al. (2023) and uncertainties in the epicentral distance of the events. Light magenta shaded windows highlight observed energy bursts consistent with potential inner core reflections.

Application to PKIKKIKP

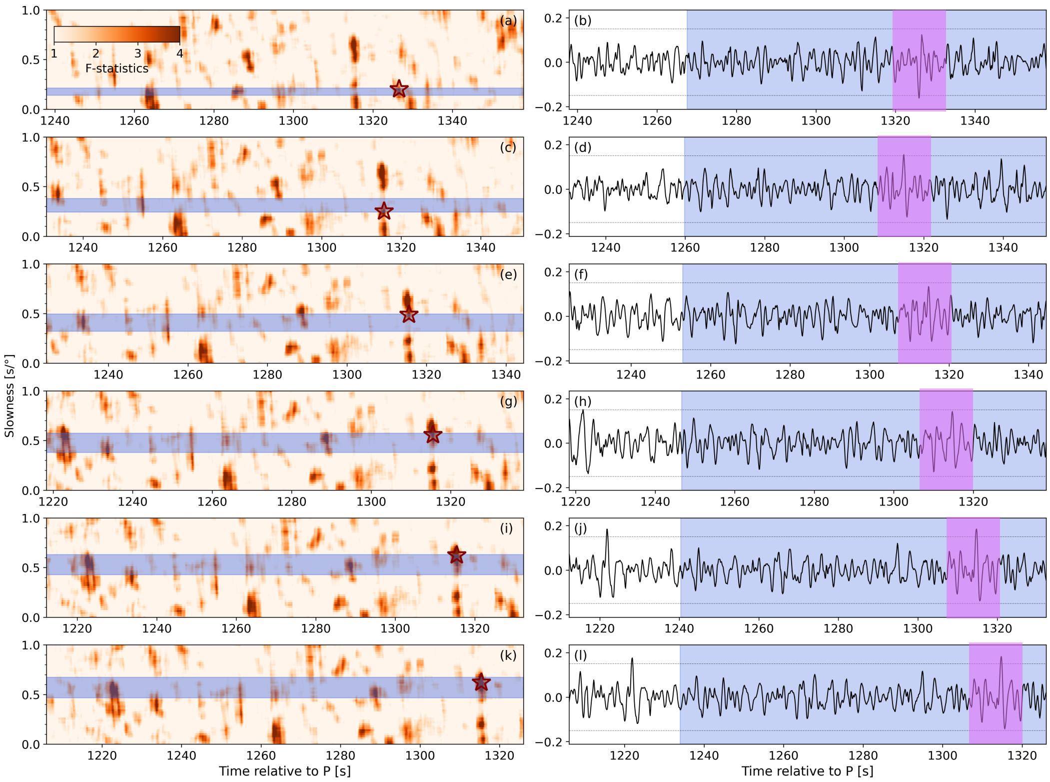

Figure S8. PKIKKIKP F-vespagram (left) and corresponding stacked waveforms (right) computed for 23 marsquakes with epicentral distances in the range 30°–40° (Table S1), assuming hypothetical inner core radii of (a-b) 100 km; (c-d) 200 km; (e-f) 300 km; (g-h) 400 km; (i-j) 500 km; and (k-l) 600 km. Inner-core P-wave velocity is assumed to be 7 km/s. On each F-vespagram, the red star denotes the picked slowness used to generate the waveform stack (righthand panels). Times are relative to the predicted P-wave arrival for the reference distance (31°) and velocity model (shown in figure 1 in the main manuscript). The light blue shading highlights the expected PKIKKIKP slowness window (horizontal blue bars, lefthand panels) and arrival time window (vertical blue bars, righthand panels) for each inner core radius, accounting for mantle variability across the velocity models of Khan et al. (2023) and uncertainties in the epicentral distance of the events. Light magenta shaded windows highlight observed wave packets consistent with potential PKIKKIKP arrivals.

References

InSight Marsquake Service. (2023). *Mars seismic catalogue, insight mission; v14 2023-04-01.* ETHZ, IPGP, JPL, ICL, Univ. Bristol. Retrieved from `https://www.insight.ethz.ch/seismicity/catalog/v14` doi: 10.12686/a21

Khan, A., Huang, D., Durán, C., Sossi, P. A., Giardini, D., & Murakami, M. (2023). Evidence for a liquid silicate layer atop the Martian core. *Nature*, *622*(7984), 718-723. doi: 10.1038/s41586-023-06586-4